Fréedericksz Transitions in Crossed Electric and Magnetic Fields

G. Barbero, E. Miraldi, C. Oldano, and P. Taverna Valabrega

Dipartimento di Fisica, Politecnico di Torino, Torino, Italia
and CISM, Unità del Politecnico di Torino

Z. Naturforsch. **43a**, 547–554 (1988); received January 23, 1988

A homogeneously aligned nematic layer with positive dielectric and diamagnetic anisotropies, placed in crossed electric and magnetic fields orthogonal to the undistorted molecular direction, is considered. Following Deuling's procedure, the possible director field configurations are classified into four types or "phases", characterized by distortions which are zero, pure twist, splay-bend and mixed type, respectively. It is shown that the transitions between these phases are generally of second order. Simple approximate expressions relating the critical fields and the distortion angles are given for the limiting cases of very small and very large distortions. The validity ranges of the approximations are found by comparison with the results of a numerical analysis. The experimental critical lines corresponding to three different types of phase transitions, obtained with a ZLI 1738 sample, are compared with theoretical ones. The agreement between theory and experiment is quite satisfactory.

PACS 61.30-v

1. Introduction

The first and second order transitions for the molecular orientation in a liquid crystal film, induced by an external field (Fréedericksz transitions), have received a great deal of interest in recent years. New types of transitions have been discovered, such as the transition giving rise to a periodic distortion [1, 2] and the one induced by an optical field [3, 4]. Great emphasis is given to the effects obtained by applying a new field, orthogonal or parallel to the previous one [5, 6]. From an applicative point of view the new field plays the role of a control parameter, which may enhance the optical response and reduce the transition times of a liquid crystal display. In the framework of the theory of critical phenomena the maximum orientation angle can be treated as an order parameter whose conjugate intensive variable is the distorting field. In general, the additional field plays the role of an intensive variable not conjugated to the order parameter, which may change the critical point into a critical line and give rise to multicritical points. We notice that the above transitions are relatively simple to observe experimentally and to treat analytically, as compared with other critical phenomena, but much more complex, from both points of view, than the transitions originally considered by Fréedericksz.

In this paper we consider an experiment which is nearly as simple to perform as the original Fréedericksz transitions. It gives rise to different types of phase transitions, which are as interesting, or more, than the above mentioned ones (at least from the point of view of the theory of critical phenomena). The set-up consists of a single-crystal nematic layer subjected to a dc magnetic field $\boldsymbol{H}$ and a low frequency electric field $\boldsymbol{E}$, such that $\boldsymbol{H}, \boldsymbol{E}$ and the undistorted director (direction of molecular alignment) $\boldsymbol{n}_0$ are mutually orthogonal. The nematic has positive diamagnetic and dielectric anysotropies $\varepsilon_a = \varepsilon_{\parallel} - \varepsilon_{\perp}$ and $\chi_a = \chi_{\parallel} - \chi_{\perp}$, where χ and ε are the magnetic susceptibility and dielectric tensors, respectively, and where parallel and perpendicular refer to the direction of $\boldsymbol{n}$. The two fields, separately, would give distortions in two mutually orthogonal planes, and the corresponding maximum distortion angles can be considered as two different order parameters. The two distortions are detected by measuring the transmitted intensity of a light beam at normal incidence, with the sample between crossed polarizers.

This case was first considered by Deuling et al. [7], and has yet received little attention [8, 9]. Our interest in this experiment is due to the following reasons.

– The experiment allows to measure many parameters (in particular the Frank elastic constants K_{11}, K_{22}, K_{33}) with a unique sample and without any

Reprint requests to Dr. G. Barbero, Dipartimento di Fisica, Politecnico di Torino, C. so Duca degli Abruzzi, 24, I-10129 Torino/Italien.

0932-0784 / 88 / 0600-0547 $ 01.30/0. – Please order a reprint rather than making your own copy.

change of the experimental apparatus. If the surface treatment is such that it gives weak anchoring, it offers a way to measure the anchoring energy as a function of the two angles which define the molecular direction at the surface.

– With a suitable choice of the material parameters and of the field strengths, different types of transitions can occur, which are of great interest from the point of view of the theory of critical phenomena and for the possible applications to electro-optic devices.

The main purpose of this paper is to complete the analysis of refs. [7–9] and to obtain a sound theoretical basis for the experiment. In particular, we obtain some very simple approximate expressions, which relate the two fields with the corresponding order parameters in the extreme cases of very small and very large distortions, and compare them with the exact ones, obtained numerically, and with the experimental data. For the sake of simplicity, only the steady state for the aperiodic distortion in strong anchoring conditions is considered.

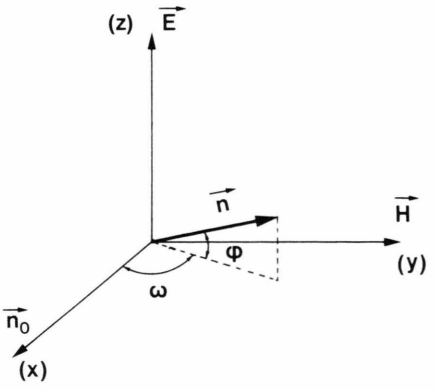

Fig. 1. Reference frame used in our analysis. The undistorted nematic is in planar configuration. ω (twist) and ϕ (splay + bend) are the polar angles characterizing the nematic director $\boldsymbol{n}$.

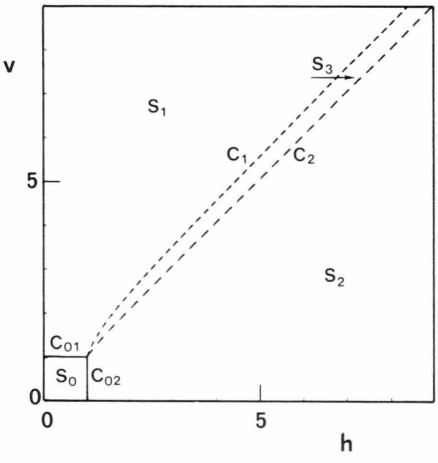

Fig. 2. Phase diagram of a planar nematic layer in crossed electric and magnetic fields. The region S_0 corresponds to the undistorted configuration; the regions S_1, S_2, S_3 correspond to splay-bend, twist and general type distortions, respectively. The material parameters are $K_{11} = K_{22} = 4.6 \times 10^{-7}$ dyne, $K_{33} = 8 \times 10^{-7}$ dyne, $\varepsilon_{\parallel} = 19.3$, $\varepsilon_{\perp} = 6$; h is the reduced magnetic field and v the reduced voltage.

2. Theory

Let the nematic substance be confined between the planes $z = \pm d/2$ of a Cartesian coordinate system. The treatment of the boundary surfaces gives an uniform alignment, with the director in the x-direction and with the strong anchoring. The electric and magnetic fields are parallel to the axes z and y, respectively. Since only aperiodic distortions are considered, the director field does not depend on the coordinates x and y, i.e. $\boldsymbol{n} = \boldsymbol{n}(z)$. In the notations of [7], $n = (\cos\phi \cos\omega, \cos\phi \sin\omega, \sin\phi)$, where the angles ω and ϕ are defined in Fig. 1, and the free energy per unit area is given by

$$G = (\pi/d) \left\{ \frac{1}{2} \int_{-\pi/2}^{\pi/2} [(K_{11} \cos^2\phi + K_{33} \sin^2\phi)\, \dot{\phi}^2 + (K_{22} \cos^2\phi + K_{33} \sin^2\phi) \cos^2\phi\, \dot{\omega}^2 - K_{22} h^2 \cos^2\phi \sin^2\omega]\, \mathrm{d}u - \frac{d}{8\pi^2} D_z V \right\}, \tag{1}$$

where $u = (\pi/d) z$ is a reduced coordinate, the dot means derivation with respect to u and $h = H/H_{c2}$ is the reduced magnetic field, where

$$H_{c2} = (\pi/d) \sqrt{K_{22}/\chi_a} \tag{2}$$

is the threshold magnetic field for the Fréedericksz transition in the absence of the electric field;

V is the applied voltage and D_z the z-component of the electric displacement; D_z is constant across the sample and given by [10]

$$D_z = (\pi/d)\, V \left\{ \int_{-\pi/2}^{\pi/2} (\varepsilon_{\parallel} \sin^2\phi + \varepsilon_{\perp} \cos^2\phi)^{-1}\, \mathrm{d}u \right\}^{-1}. \tag{3}$$

By minimizing the free energy with respect to $\omega(u)$ and $\phi(u)$, one obtains the differential equations [7]

$$\frac{\mathrm{d}}{\mathrm{d}u}\{(K_{22}\cos^2\phi + K_{33}\sin^2\phi)\cos^2\phi\,\dot{\omega}\} + K_{22}h^2\cos^2\phi\sin\omega\cos\omega = 0, \tag{4}$$

$$\frac{\mathrm{d}}{\mathrm{d}u}\{(K_{11}\cos^2\phi + K_{33}\sin^2\phi)\dot{\phi}\} = (K_{33}-K_{11})\sin\phi\cos\phi\,\dot{\phi}^2 + \frac{1}{2}\dot{\omega}^2\frac{\mathrm{d}}{\mathrm{d}\phi}\{\cos^2\phi\,(K_{22}\cos^2\phi + K_{33}\sin^2\phi)\}$$

$$+ K_{22}h^2\sin^2\omega\sin\phi\cos\phi - \frac{d}{8\pi^2}D_z^2\frac{\varepsilon_a\sin\phi\cos\phi}{(\varepsilon_{\parallel}\sin^2\phi + \varepsilon_{\perp}\cos^2\phi)^2}\,. \tag{5}$$

The functions $\omega(u)$ and $\phi(u)$ are obtained by a numerical integration of these equations with the boundary conditions

$$\phi(\pm\pi/2) = \omega(\pm\pi/2) = 0. \tag{6}$$

As expected, ϕ and ω are even functions of u and reach their maximum values ϕ_M, ω_M at $z = u = 0$. The angles ϕ_M and ω_M are treated as order parameters. This suggest to classify the solutions into four types:

S_0) $\phi_M = \omega_M = 0$, i.e. no distortion;
S_1) $\phi_M \neq 0$ and $\omega_M = 0$, i.e. splay-bend distortion;
S_2) $\phi_M = 0$ and $\omega_M \neq 0$, i.e. twist distortion;
S_3) $\phi_M \neq 0$ and $\omega_M \neq 0$, i.e. splay-bend and twist distortions.

The four types of solutions, or "phases", correspond to four regions of the h, v plane. Here v is the reduced voltage, namely the ratio V/V_{c1}, where

$$V_{c1} = 2\pi\sqrt{\pi K_{11}/\varepsilon_a} \tag{7}$$

is the threshold voltage at zero magnetic field.

Figure 2 shows the "phase diagram" for the following set of parameters values: $K_{11} = K_{22} = 4.6 \times 10^{-7}$ dyne, $K_{33} = 8 \times 10^{-7}$ dyne, $\varepsilon_{\parallel} = 19.3$, $\varepsilon_{\perp} = 6$, $\chi_a = 10^{-7}$. With this choice of parameters all the transitions between different phases are of the second order, and give rise to four critical lines, which start or terminate in the unique singular point $h = v = 1$.

The phase diagram, shown in Fig. 2, is very similar to the one reported by Deuling [8]. In both cases, all types of solutions are stable. However, with a different choice of the parameters the two boundary lines C_1 and C_2 of the domain S_3 may have a second intersection point. Therefore this domain splits into two separate regions. In one of the these regions solutions of type S_1, S_2 and S_3 coexist, with the latter ones unstable. In this case phenomena such as first order transitions, bistability and hysteresis are expected.

2.1. *Approximate Analysis for Small Distortions*

An analytic approximate expression for $v_1 = f_1(h)$, which gives the correct slope of the curve C_1 in the singular point, is given in [9]. It has been obtained by approximating (5) with the Mathieu equation. Here we give a simpler method to obtain the exact values of the critical fields and the correct initial slope of both curves C_1 and C_2. The starting point is to insert in the expression of the free energy G, given by (1) and (3), the approximate expressions

$$\phi(u) = \phi_M\cos u; \quad \omega(u) = \omega_M\cos u \tag{8}$$

and to expand $G = \pi\tilde{G}(\phi_M, \omega_M)/(4d)$ up to fourth order terms in ϕ_M and ω_M. This gives

$$\tilde{G} = K_{11}(1-v^2)\phi_M^2 + K_{22}(1-h^2)\omega_M^2 + \frac{1}{4}\left\{\left(K_{33} - K_{11} + K_{11}\frac{\varepsilon_{\parallel}}{\varepsilon_{\perp}}v^2\right)\phi_M^4 + (K_{33} - 2K_{22} + 3K_{22}h^2)\phi_M^2\omega_M^2 + K_{22}h^2\omega_M^4\right\}. \tag{9}$$

The equilibrium configurations are the minima of the function $\tilde{G}(\phi_M,\omega_M)$, and are given by

$$\frac{\partial\tilde{G}}{\partial\phi_M} = \frac{\partial\tilde{G}}{\partial\omega_M} = 0, \tag{10}$$

$$\frac{\partial^2\tilde{G}}{\partial\omega_M^2} > 0, \quad \frac{\partial^2\tilde{G}}{\partial\phi_M^2}\cdot\frac{\partial^2\tilde{G}}{\partial\omega_M^2} - \left(\frac{\partial^2\tilde{G}}{\partial\phi_M\,\partial\omega_M}\right)^2 > 0. \tag{11}$$

By straightforward calculations one obtains the following results:

i) The S_0-type solutions, given by $\phi_M = \omega_M = 0$, are stable if and only if $v < 1$, $h < 1$.

ii) The S_1-type solutions are given by

$$\phi_M^2 = \frac{4K_{11}}{K_{33} + K_{11}(\varepsilon_a/\varepsilon_{\perp})}(v-1) + O[(v-1)^2];$$
$$\omega_M = 0 \tag{12}$$

and are stable if

$$v > v_1 = 1 + 2\,\frac{K_{22}}{K_{33}+K_{22}} \cdot \frac{K_{11}}{K_{33}+K_{11}(\varepsilon_a/\varepsilon_\perp)}(h-1) + O[(h-1)^2]. \tag{13}$$

iii) The S_2-type solutions are given

$$\phi_M = 0;\ \omega_M^2 = 4(h-1) + O[(h-1)^2] \tag{14}$$

and are stable if

$$v < v_2 = 1 + \frac{K_{33}+K_{22}}{2K_{11}}(h-1) + O[(h-1)^2]. \tag{15}$$

In (12–15) only the terms linear in $(h-1)$ and $(v-1)$ have been explicitly written, since the higher order terms are not correct. This fact is a direct consequence of the approximation given by (8). In Fig. 3 the functions $\phi_M(v)$ and $\omega_M(h)$ given by (12) and (14), are compared with the exact ones, obtained by a numerical integration of (4) and (5). A similar comparison for the functions $v_1(h)$ and $v_2(h)$ is shown in Figure 4. The two figures show that the approximate expressions give the correct initial slope of the curves, and that they practically coincide with the exact ones up to angles ϕ_M and ω_M of the order of 0.3 rad.

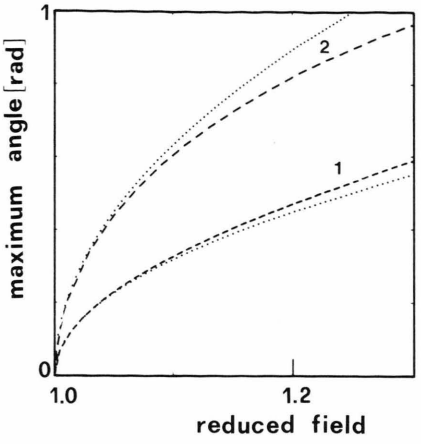

Fig. 3. Plots of the approximate (dotted lines) and exact (dashed lines) expression of $\phi_M(h)$ and $\omega_M(v)$ corresponding to splay-bend (1) and twist (2) distortions, respectively, for the same parameters of Figure 2.

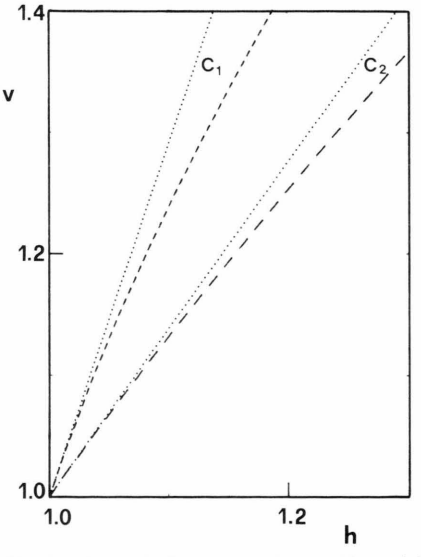

Fig. 4. Plots of the approximate (dotted lines) and exact (dashed lines) expressions of the functions $v_1(h)$ and $v_2(h)$ giving the critical lines C_1 and C_2, respectively, for the same parameters of Figure 2.

2.2. *Approximate Analysis for Very Strong Distortions*

An approximate expression for the curve C_2, valid in the limit $h \gg 1$, is given in [7], and reads

$$v_2^2 = 1 + (K_{22}/K_{11})h^2. \tag{16}$$

It was obtained by assuming $\omega(u) = \pi/2$ (as it is well known, in the above limit $\omega(u)$ is very close to $\pi/2$ except for two boundary layers, whose thickness is of the order of magnitude of the magnetic coherence length) and $\phi(u) = \phi_M \cos u$.

A similar procedure may be used to obtain the curve C_1 in the limit $v \gg 1$. However, it is necessary to identify the direction of $\boldsymbol{n}$ with angles different from ϕ and ω. In fact a simple inspection of (1) shows that for $\phi = \pi/2$ the dependence of $\tilde{G}$ on ω disappears.

Let us write $\boldsymbol{n}$ as

$$\boldsymbol{n} = (\cos\alpha\,\cos\beta,\ \sin\alpha,\ \cos\alpha\,\sin\beta), \tag{17}$$

where α is the angle of $\boldsymbol{n}$ with the (x, z) plane and β the angle between the x-axis and the projection of $\boldsymbol{n}$ on the same plane.

In the limit $v \gg 1$ and for splay-bend distortions, β is nearly everywhere close to $\pi/2$. By assuming $\beta = \pi/2$, the free energy becomes

$$\tilde{G} = \frac{1}{2}K_{33}\int_{-\pi/2}^{\pi/2}\left(\dot{\alpha}^2 + \frac{K_{11}v^2 - K_{22}h^2}{K_{33}}\alpha^2\right)\mathrm{d}u + \text{const.} \tag{18}$$

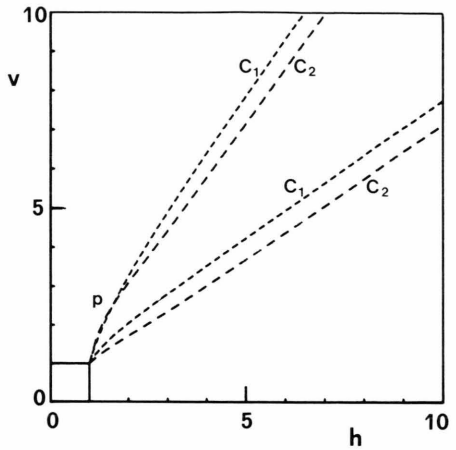

Fig. 5. Plot of the critical lines C_1, C_2 for two different values of the ratio K_{11}/K_{22}, i.e. for $K_{22} = 1.8 \times 10^{-7}$ dyne, $K_{11} = \frac{1}{2} K_{22}$ (upper curves) and $K_{22} = 2.7 \times 10^{-7}$ dyne, $K_{11} = 2 K_{22}$ (lower curves). The other parameters are the same as in Figure 2.

The solution with $\alpha = 0$ is stable with respect to fluctuations of the type $\alpha(u) = \alpha_M \cos u$ if

$$v^2 < v_1^2 = (K_{33}/K_{11}) + (K_{22}/K_{11}) h^2 . \tag{19}$$

In the limit $h \to \infty$, (16) and (19) coincide and become

$$v_1 \simeq v_2 \simeq \sqrt{K_{22}/K_{11}}\, h . \tag{20}$$

In this limit, the lines C_1 and C_2 become parallel straight lines with slope $(K_{22}/K_{11})^{1/2}$, in agreement with Fig. 2, where $K_{22}/K_{11} = 1$. In Fig. 5 we have plotted the lines C_1 and C_2 obtained with the same values of K_{33}, $\varepsilon_{\|}$ and $\varepsilon_{\perp}$ and with two different values of K_{22}/K_{11}. The plot shows that (20) gives the correct asymptotic behaviours, which are reached, for all practical purposes, for $h \gtrsim 5$.

Incidentally, we notice that the initial parts of the upper curves C_1 and C_2 nearly coincide, and that they intersect in a point P. This point corresponds to a first order transition between a splay-bend and a twist distortion.

2.3. Some Considerations on the Flexoelectric Effect

In our analysis we have neglected the flexoelectric effect. Since the frequency of the applied voltage is of the order of 1 kHz, there is no direct coupling between the flexoelectric polarization and the applied electric field.

But as shown in [11, 12] a nematic distortion gives rise to a flexoelectric polarization, which produces a back electric field. The coupling between this electric field and the flexoelectric polarization gives a dielectric energy which depends on the square of the deformation gradient and has therefore the same structure of the elastic energy [11, 12]. If we take into account the flexoelectric polarization, the first term in (1) becomes

$$\left\{ K_{11} \cos^2\phi + K_{33} \sin^2\phi + \pi \frac{(e_{11} + e_{33})^2}{\varepsilon_{\|} \sin^2\phi + \varepsilon_{\perp} \cos^2\phi} \sin^2(2\phi) \right\} \dot{\phi}^2 , \tag{21}$$

while the other terms do not change. In (21) e_{11} and e_{33} are the flexoelectric coefficients [13]. This equation shows that, in the a.c. regime, the flexoelectric properties of the nematic introduce only a renormalization of the splay and bend elastic constants [11, 12]. Equation (21) is obtained by assuming that the nematic is a perfect insulator; hence it holds only if Debye's screening length L_D is greater than the distance where the $\phi(z)$-variation occurs [14]. For typical concentrations of impurities L_D is smaller than 1 μm [15]. Consequently near the $v = h = 1$ point, where $\phi(z)$ changes over the sample thickness, the nematic can be considered as a conductor. It follows that the last term in (21) is absent, since the flexoelectric polarization charges are completely screened by ionic conductivity [15].

For the same reasons the curve C_2 is not affected when the flexoelectricity effect is neglected.

On the contrary, the curve C_1 may change when the $\phi(z)$-deformation is localized on a thickness smaller than L_D. Anyway in our experiment the maximum reduced voltage v is of the order of 4. Therefore the electric coherence length $\xi_E = (d/\pi) v^{-1}$ is always greater than $d/(4\pi) \sim 2$ μm. Since the $\phi(z)$-deformation takes place over $\xi_E \sim L_D$, we can still suppose that the flexoelectric polarization charges are completely screened by ionic impurity.

In the case $v \gg 1$, $\phi \sim \pi/2$ for any z, and the last term in (21) vanishes. Hence the two curves still become parallel straight-lines for $h, v \gg 1$.

3. Choice of the Experimental Set-up

In order to explain the features of the experimental set-up, we recall here the following, well known facts:

– the measure of the threshold fields for the Fréedericksz transitions has always been one of the most

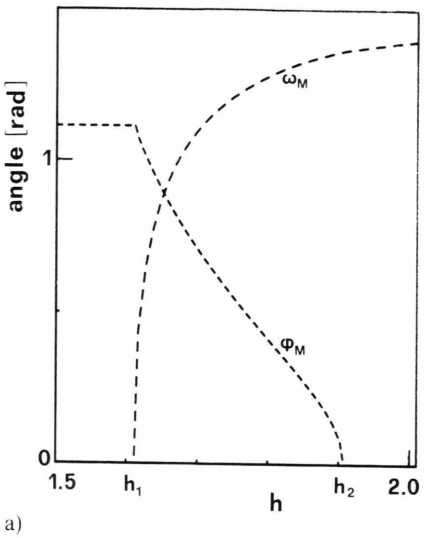

a)

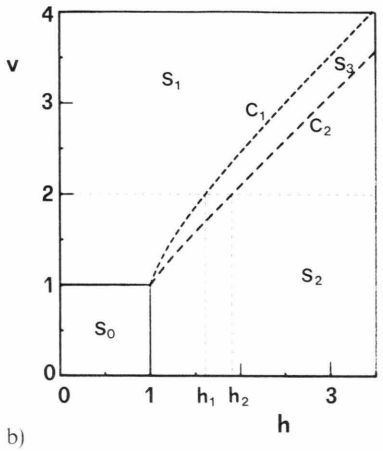

b)

Fig. 6. Fig. 6a shows a plot of $\phi_M(h)$ and $\omega_M(h)$ at constant v, when the region S_3 is crossed as shown in Fig. 6b. The material parameters are the same of Fig. 2.

widely used methods for measuring the curvature elastic constants, owing to its simplicity and accuracy; – in order to measure the three Frank elastic constants, different set-ups are generally used. In particular the onset of the pure twist distortion is not as easily detected as the other ones [16], which involve the angle ϕ and give a change in many physical quantities, (e.g. the phase difference between the ordinary and extraordinary rays for normally incident light).

For the experiment discussed in this paper, a Fréedericksz transition at any point of the curves C_{O1} and C_2 corresponds to the onset of a distortion involving

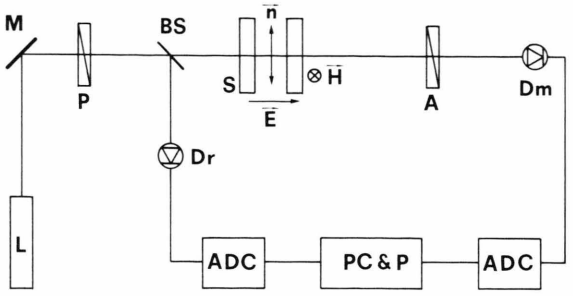

Fig. 7. Schematic drawing of the experimental set-up. The light of the laser L, via a beam stearer M, is polarized by a nicol prism P, and transmitted by the sample S and the nicol analyser A. The ratio between the intensity of the light impinging the photodiode D_m and that of the reference beam, impinging D_r via the beam splitter BS, is computed and stored in a PC via two analog to digital converters (DMA).

an abrupt change of ϕ, and is therefore easily detected. The other transitions involve a change of ω, which cannot be detected at normal incidence of light, for the adiabatic theorem [17]. For a point of the curve C_{O2}, the angle ϕ remains equal to zero, whereas for a point of the curve C_1 the ϕ-change is not yet known. Its knowledge is crucial from the point of view of the transition detection. In Fig. 6a, a plot of ϕ_M and ω_M vs. h is given, when the domain corresponding to splay-bend and twist is crossed at constant v, as shown in Figure 6b. In correspondence of both transition points an abrupt change occurs for $\phi_M(h)$ as well as for $\omega_M(h)$. This means that any point of the three critical curves C_{O1}, C_2, C_3 can be very easily and precisely detected by measuring a unique quantity, as e.g. the transmittance of the sample between crossed polarizers at normal incidence of light.

The experimental set-up used in our experiments is shown in Figure 7. The beam splitter is used to obtain a reference signal, in order to correct the intensity fluctuations of the laser beam [18].

The sample is a 23 μm film of ZLI 1738, placed between conductively coated glass plates in the following way: i) the glasses are rinsed in chromic mixture and washed in bidistilled water, ii) they are dipped in an ethanol solution of silan (EMAP by Chisso Coorp.) and dryed at 120 °C for half an hour, iii) they are strongly rubbed with teflon. The two glasses are kept parallel with mylar spacers under very small mechanical pressure, in order to avoid birefringence induced by stresses.

The surface treatment insures a reasonably strong anchoring for twist deformation and, probably, also

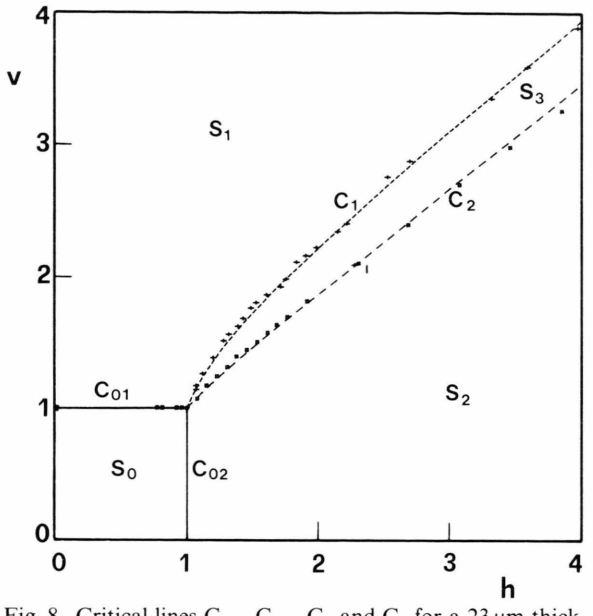

Fig. 8. Critical lines C_{01}, C_{02}, C_1 and C_2 for a 23 μm thick layer of ZLI 1738 at 18°. The best fit lines are obtained with $K_{11} = 7.6 \times 10^{-7}$ dyne, $K_{22}/K_{11} = 0.7$, $K_{33}/K_{11} = 1.4$, $\varepsilon_{\parallel} = 19.3$, $\varepsilon_{\perp} = 6$. The threshold for the pure twist distortion (line C_{02}), is obtained experimentally on the basis of a unique point, i.e. the intersection point of the four lines.

for splay-bend deformation. In fact, with a magnetic field $H \sim 20$ KG (i.e. $h \sim 7$) the nematic surface rotation is smaller than 5° [18].

4. Experimental Results and Discussion

As explained in Sect. 3, with our experimental set-up we are able to measure the critical fields corresponding to any point of the curves C_{01}, C_1 and C_2 of Figure 2. Measurements have been done on the 23 μm thick ZLI 1738 sample at 18 °C. The data are plotted in Figure 8. The points of the curves C_{01} and C_2 are obtained by increasing the voltage V at fixed H. The critical value V_2 of V corresponds to the onset of a series of maxima and minima for the transmitted light beam, due to the interference between the ordinary and extraordinary rays within the sample. In fact, the angle ϕ_M is zero for $v < v_2$ and increases as $(v - v_2)^{1/2}$ for $V \gtrsim V_2$.

The points of the curve C_1 are obtained by increasing the magnetic field H at fixed V. Also in this case the critical value of H corresponds to the onset of a series of maxima and minima of interference, since in these experimental conditions ϕ_M is constant for $h < h_2$ and abruptly begins to decrease for $h > h_1$ (see Figure 6a).

The uncertainties in the measurements of H_c are shown in the Fig. 8, and are mainly due to difficulties in the magnetic field control. For the same reason we were not able to detect with reasonable accuracy the critical field h_2, corresponding to a point of the curve C_2, where a further abrupt change of the derivative $d\phi_M/dh$ occurs. The best fit curves of Fig. 8 have been obtained by assuming $\varepsilon_{\parallel} = 19.3$, $\varepsilon_{\perp} = 6$ [19] and correspond to $K_{11} = 7.6 \times 10^{-7}$, $K_{22} = 0.7 \times K_{11}$, $K_{33} = 1.4 \times K_{11}$. More precisely:

- K_{11} has been obtained from the points of the curve C_{01}, where an initially pure splay distortion occurs;
- the ratio K_{22}/K_{11} is essentially determined by the points of the upper portion of the curves C_1 and C_2, and is found to be 0.70 ± 0.03;
- the ratio K_{33}/K_{11} is determined by the initial slope of the curves C_1 and C_2, and is found to be 1.4 ± 0.10.

One may notice that the accuracy of the present measurement of K_{11} and K_{22} is the same as with previous methods, but the detection technique is simple, at least for K_{22}. The accuracy of K_{33}-value is worse, at least with the present apparatus. However, our main interest in this experiment is not the measurement of the Frank elastic constants, but the experimental verification of the theory. As we can see from Fig. 8, the agreement between experiment and theory is quite satisfactory. Incidentally, we observe that the critical line C_1 was predicted and experimentally obtained for the first time with p-p-dibutylazoxybenzene by Deuling et al. [20].

To conclude, we note the following features of this experiment which are, in our opinion, very important and are presently under further investigation:

1) A simple inspection of Figs. 2 and 5 shows that for $H \geq H_{c2}$ a drastic change of the molecular alignment occurs for a small change ΔV of the applied voltage. The quantity ΔV may be further decreased and possibly reduced to zero, by a suitable choice of the material parameters and of the surface treatment. This gives a bistable or nearly bistable behaviour for the optical properties of the sample.
2) In weak anchoring conditions, the experiment allows to measure the surface torques of the boundary surfaces on the nematic as a function of the two angles which define the surface molecular alignment.

[1] F. Lonberg and R. B. Meyer, Phys. Rev. Lett. **55,** 718 (1985).
[2] U. D. Kini, J. Physique **47,** 693 (1986); **47,** 1829 (1986) and **48,** 1187 (1987); – E. Miraldi, C. Oldano, and A. Strigazzi, Phys. Rev. A **34,** 4398 (1986); W. Zimmermann and L. Kramer, Phys. Rev. Lett. **56,** 1655 (1986).
[3] A. S. Zolot'ko, V. F. Kitaeva, N. Kroo, N. N. Sobolev, and L. Chilag, Zh. Eksp. Teor. Fiz. Pis'ma Red **32,** 170 (1980) (JEPT Lett. **32,** 158 (1980)); B. Ya. Zel'dovich, N. V. Tabiryan, and Yu. S. Chilingaryan, Zh. Eksp. Teor. Fiz. **81,** 72 (1981) (Sov. Phys. – JEPT **54,** 32 (1981)); B. Ya. Zel'dovich and N. V. Tabiryan, Zh. Eksp. Teor. Fiz. **79,** 2388 (1980) (Sov. Phys. – JEPT **52,** 1210 (1980)).
[4] S. D. Durbin, S. M. Arakelian, and Y. R. Shen, Phys. Rev. Lett. **47,** 1411 (1981); H. L. Ong, Phys. Rev. A **28,** 2393 (1983); Y. L. Shen, Phil. Trans. Roy. Soc. London A **313,** 327 (1984).
[5] H. M. Zenginoglou, J. Physique **48,** 1599 (1987).
[6] H. L. Ong, Phys. Rev. A **31,** 3450 (1985) and **33,** 3550 (1986); Appl. Phys. Lett. **46,** 822 (1985).
[7] H. J. Deuling, E. Guyon, and P. Pieranski, Solid State Comm. **15,** 277 (1974).
[8] H. J. Deuling, in Solid State Physics, Suppl. 14 edited by L. Liebert, Academic Press, London 1978.
[9] G. Barbero and A. Strigazzi, Z. Naturforsch **39a,** 571 (1984).
[10] H. J. Deuling, Mol. Cryst. Liq. Cryst. **19,** 123 (1972).
[11] W. Helfrich, Mol. Cryst. Liq. Cryst. **26,** 1 (1974).
[12] H. J. Deuling, Mol. Cryst. Liq. Cryst. **26,** 281 (1974) and Solid State Commun. **14,** 1073 (1974).
[13] R. B. Meyer, Phys. Rev. Lett. **22,** 918 (1969).
[14] G. Barbero and G. Durand, J. Physique **47,** 2129 (1986).
[15] L. M. Blinov, Electro-optical and Magneto-optical Properties of Liquid Crystals, J. Wiley and Sons, Chichester 1983, p. 161.
[16] P. E. Cladis, Phys. Rev. Lett. **28,** 1629 (1972).
[17] G. Maughin, Phys. Z. **12,** 1011 (1911); see also P. G. de Gennes, The Physics of Liquid Crystals, Oxford University Press, London 1975.
[18] G. Barbero, E. Miraldi, C. Oldano, M. L. Rastello, and P. Taverna Valabrega, J. Physique **47,** 1411 (1986).
[19] The data $\varepsilon_{\parallel} = 19.3$, $\varepsilon_{\perp} = 6$ relative to ZLI 1738 are reported in Merck liquid crystals catalogue 1985.
[20] H. J. Deuling, A. Buka, and J. Janossy, J. Physique **37,** 965 (1976).